AD NUMBER

AD443680

LIMITATION CHANGES

TO:

Approved for public release; distribution is unlimited.

FROM:

**Distribution authorized to U.S. Gov't. agencies and their contractors;
Administrative/Operational Use; JUN 1964. Other requests shall be referred to Office of Naval Research, Washington, DC 20360.**

AUTHORITY

onr ltr, 4 may 1977

[redacted]

[redacted]

[redacted]

CORNING
CORNING GLASS WORKS

SEMIANNUAL TECHNICAL REPORT

January 1964 to June 1964

Contract No. Nonr - 3833(00)

June 30, 1964

Glass Laser Research

Corning Glass Works

Corning, New York

Order No. 306-62

Project Code No. 7300

Authors:

M. L. Charters

N. F. Borrelli

P. E. Gordon

R. D. Maurer

ABSTRACT

Measurement of relevant physical properties has continued. The technique for measuring absorption loss at 1.06μ has been improved to obtain reliable data from glasses that are not of optical quality. Experimental equipment has been set up to obtain the optical path change with temperature at 1.06μ. The theory of crystal field effects on the fluorescence of Nd^{3+} is examined and correlation between lifetime and optical absorption pointed out. An analysis is presented of the absorbed energy distribution in a cylindrical laser rod.

This work was partially supported by Project DEFENDER under the joint sponsorship of the Advanced Research Projects Agency, the Office of Naval Research and the Department of Defense.

TABLE OF CONTENTS

FIGURES

I. PHYSICAL PROPERTIES OF GLASS FOR LASERS

1. Absorption Loss Measurements at 1.06 Microns

The performance of glass lasers depends critically upon the internal absorption of energy. This energy loss can result from different mechanisms in the laser but one important cause is the conventional, quiescent absorption of light at the laser wavelength. Special apparatus has been set up to measure this quantity since no commercial spectrophotometer can reliably measure optical absorptions as low as those encountered. The equipment and its use with optically perfect laser glass was described in the last report. Below we describe how this method has been extended and improved to measure absorption in somewhat poorer optical quality glass melts.

The measurement of laboratory melted samples requires a somewhat different approach from that used for long, high quality rods. Where excellent beam collimation was essential for long samples, it is not critical for short ones. On the other hand, the optical perfection of the long samples made beam diffusion before detection dispensable. Cordy or imperfectly polished samples, however, require the emergent beam to be well diffused to prevent changes in position or cross sectional shape from producing response changes not propotional to beam intensity. Fortunately, by substitution of collimating lenses in the light source, it is possible to trade collimation for greater beam intensity, this maintaining a reasonable signal level after diffusion.

Some glasses will absorb 0.1% or less per cm length. For a five cm length, a precision of messurement is thus required of about one part in 2000.

Although a differential method, similar to the method previously used, is indicated for the required precision, a difficulty arose in the use of the Tektronic Differential Comparator plug-in unit. The plug-in plus oscilloscope combination is extremely fast in response, about 10^{-8} seconds. The two 7102 photodetectors with associated cabling are much slower and are furthermore slightly different in response speed. This difference in transient response made the balancing of the two signals from a pulsed beam impossible and a differential method of absorption measurement using a pulsed beam was therefore not practical.

A chopped D. C. beam method was chosen to by pass these difficulties but one trouble remained; the presence of high frequency noise. This noise could possibly be suppressed by the addition of a filter. A lock-in amplifier, which acts as a very effective band pass filter, was found more satisfactory. The differential input to the lock-in is provided by a balanced input audio transformer with a grounded primary center tap. Single ended output is provided by a second identical transformer back-to-back with the first. The circuit is shown in Fig. 1.

With the lock-in amplifier, the measuring system time constant is variable by setting a dial. Noise is troublesome only if its frequency is of the order of the time constant. The optimum time constant seems to be about 0.2 sec. A considerable improvement in low frequency noise was achieved through the use of a single power supply for the two 7102 photodetectors.

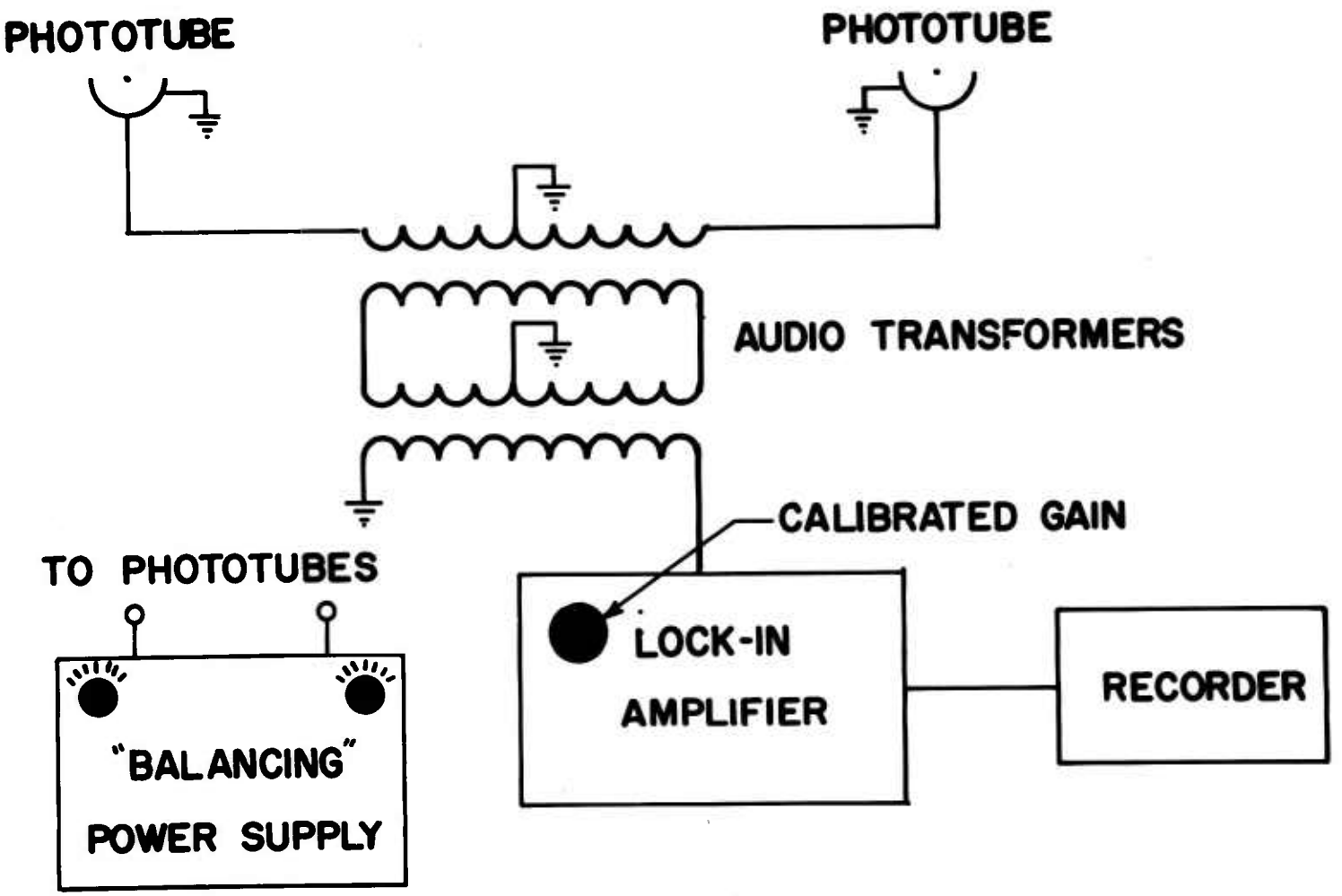

Figure 1. Absorption Loss Circuit Schematic

A diagram of the apparatus is shown in Fig. 2. The measurement procedure is now as follows. Two samples of a given glass are mounted on a slide such that the light beam can be intercepted by them alternately. The center position of the slide blocks the beam from the signal detector. The reference monitor detector sees a portion of the beam provided by a clear glass beam splitter set at 45° to the beam.

The precision of the present apparatus seems sufficient to measure a change in signal of 0.5% to within 10%, or in other words, a total absorption of $(0.5 \pm 0.05)\%$, corresponding to $0.1\%/cm \pm 0.1\%/cm$ for a five cm sample.

Although the precision of measurement seems adequate, the accuracy will depend on a completely different set of factors that have to do with the glass samples themselves and their surfaces. For a long sample of large total absorption, scattering from minute scratches, bubbles, seeds, or dirt is negligible, especially since both measurement sample and reference sample are about the same. For samples of very small total absorption, however, a slight scratch in one sample can lead to a highly precise measurement of the wrong quantity. Bubbles and seeds are therefore intolerable if no path for the beam can be found that misses them all. Since perfectly scratch-free glass surfaces are difficult to make absorption measurement accuracy on short low absorbing samples will have to rely on repeated measurements through different parts of the same samples. Samples of at least a square inch in cross section are therefore highly desirable. A rolling sample holder has been designed and built. This improvement makes the averaging of sample defect errors more or less automatic.

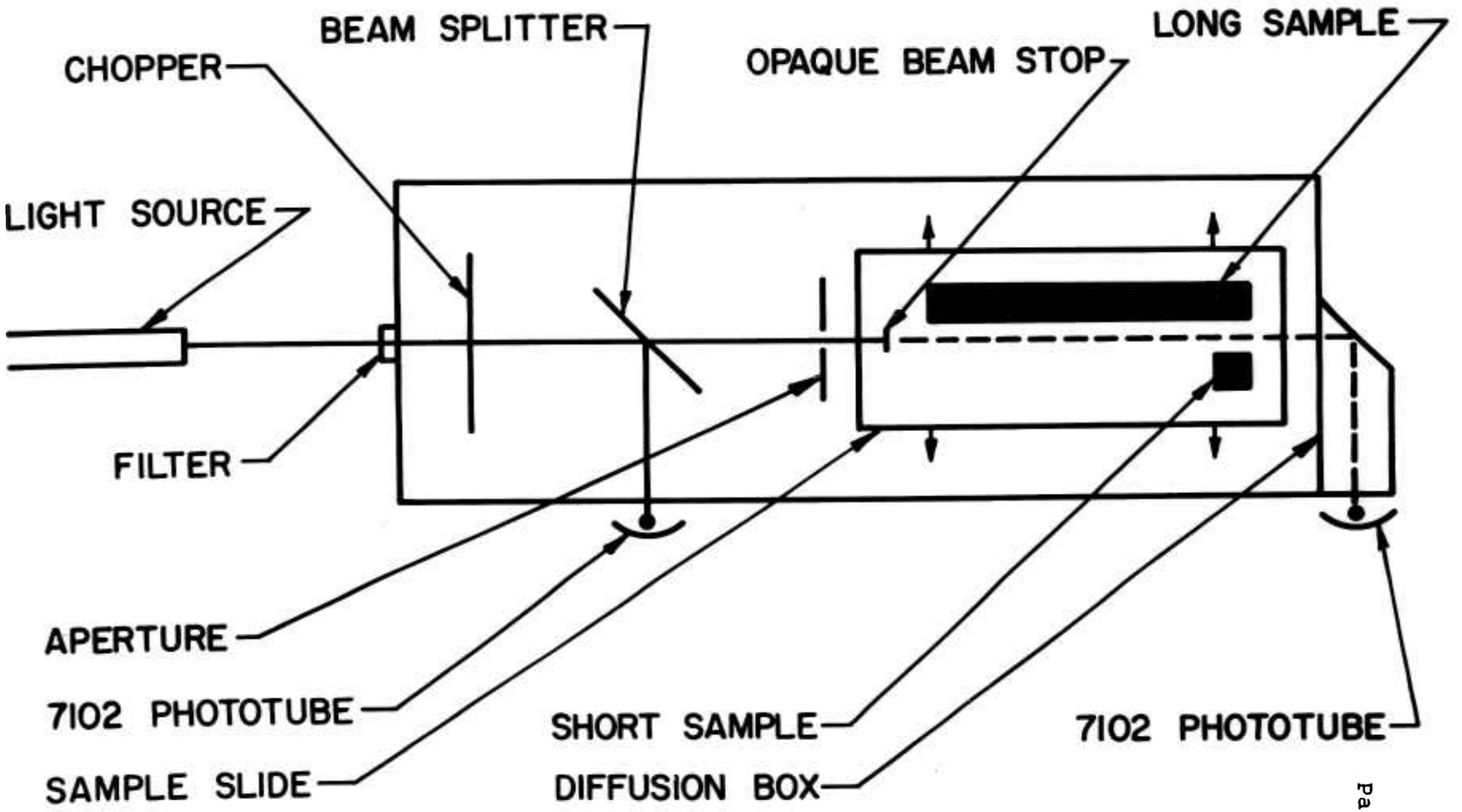

Figure 2. Diagram of Absorption Loss Equipment

2. Measurement of Optical Path Change with Temperature

1. Introduction

The energy absorbed in a laser rod which does not contribute to populating the $^4F_{3/2}$ state in Nd raises the temperature of the laser rod. A rise in temperature usually results in an increase in both the physical length of the rod an in its index of refraction. The combined effect produces a change in the optical path length of the rod. An analysis of these effects has been previously given.[1]

The slope of refractive index versus temperature for common glasses decreases from positive to zero to negative as the glass temperature is decreased.[2] It should be possible at a particular low temperature to make the optical path within the rod nearly constant within a small temperature interval. At a somewhat higher temperature the entire cavity can be made to retain a constant path length over a small temperature interval. The problem then, is to determine the latter temperature - the particular temperature at which the optical path change with temperature is zero.

2. The Measuring Technique

The optical path changes of concern are of the order of 1 micron, so an interferometric method is called for. The change in optical path in terms of fringes, N,observable in a laser cavity with external morrors is given by:

$$\frac{\Delta N}{\Delta T} = \frac{L}{\lambda}\left[\left(\frac{dn}{dt} + n\alpha\right) - \alpha\right]$$

for a single-pass, or $\frac{2L}{\lambda}\left[---\right]$ for a double-pass instrument, where

ΔN = fringe shift

ΔT = temperature change

λ = wavelength of interferometer source

$\alpha = \frac{\Delta L}{L}$

The determination of $\frac{L}{\lambda}\left(\frac{dn}{dt} + n\alpha\right)$ is experimentally both more convenient and more precise than the determination of the entire expression. There are more fringes to count per temperature interval if the measurements are made in the glass alone. An independent measurement of α of equal precision is required, however. The method described below can be used to measure the coefficient of expansion α as well, but a different sample geometry is required. An independent company funded program is underway to measure expansion coefficients to the required accuracy.

3. Apparatus

A Gaertner Scientific Corp. interferometer of the Fizeau type has been mounted so that a Helium-Neon gas laser could be substituted for its normal low pressure Hg lamp. The laser source provides several advantages. a) It provides an output at 1.15 microns -- close to the 1.06 micron neodymium wavelength. b) It also provides a 6328 Å visible output with which the system can be conveniently aligned. c) Its outputs are bright and well collimated for efficient collection by the interferometer. d) It is coherent, so long glass samples can be

used to increase measurement precision.

Figure 3 is a diagram of the present apparatus which has been constructed to test the feasibility of the method. For visual observations in the red, a microscope objective of about 8 power has been found to most efficiently diverge the laser beam to fill the aperture of the interferometer. A simple glass bead of about ¼ inch diameter taped to the aperture also works quite well, since efficiency is not a problem in the red. In order to use the infrared, however several modifications are necessary. A camera lens is substituted for the eye at the interferometer eyepiece and an image converter is placed at the focal plane of the camera. At 1.15 microns the S-1 surface of the image converter is not very sensitive, however. With the laser beam diverged to fill the optics, no fringes are visible. The microscope objective (or glass bead) must be removed. With no diverging lenses in the system, the interferometer telescope objective focuses the laser beam to a pinpoint on the sample surface. The pinpoint of light is visible on the image converter but fringe movement is detectable only as a change of spot intensity -- no direction of fringe motion is detectable. In order to expand the spot size slightly but still confine the beam to a small area, a 20 inch focal length lens is inserted in the laser beam. It is moved to a position that enlarges the beam at the sample just enough to resolve a fringe and its direction of motion. The spot is still intense enough to be visible on the image converter.

To reach liquid N_2 temperatures, the sample, with a copper-constantan thermocouple attached, is mounted in a glass container as shown in Fig. 3. The container is evacuated to prevent sample

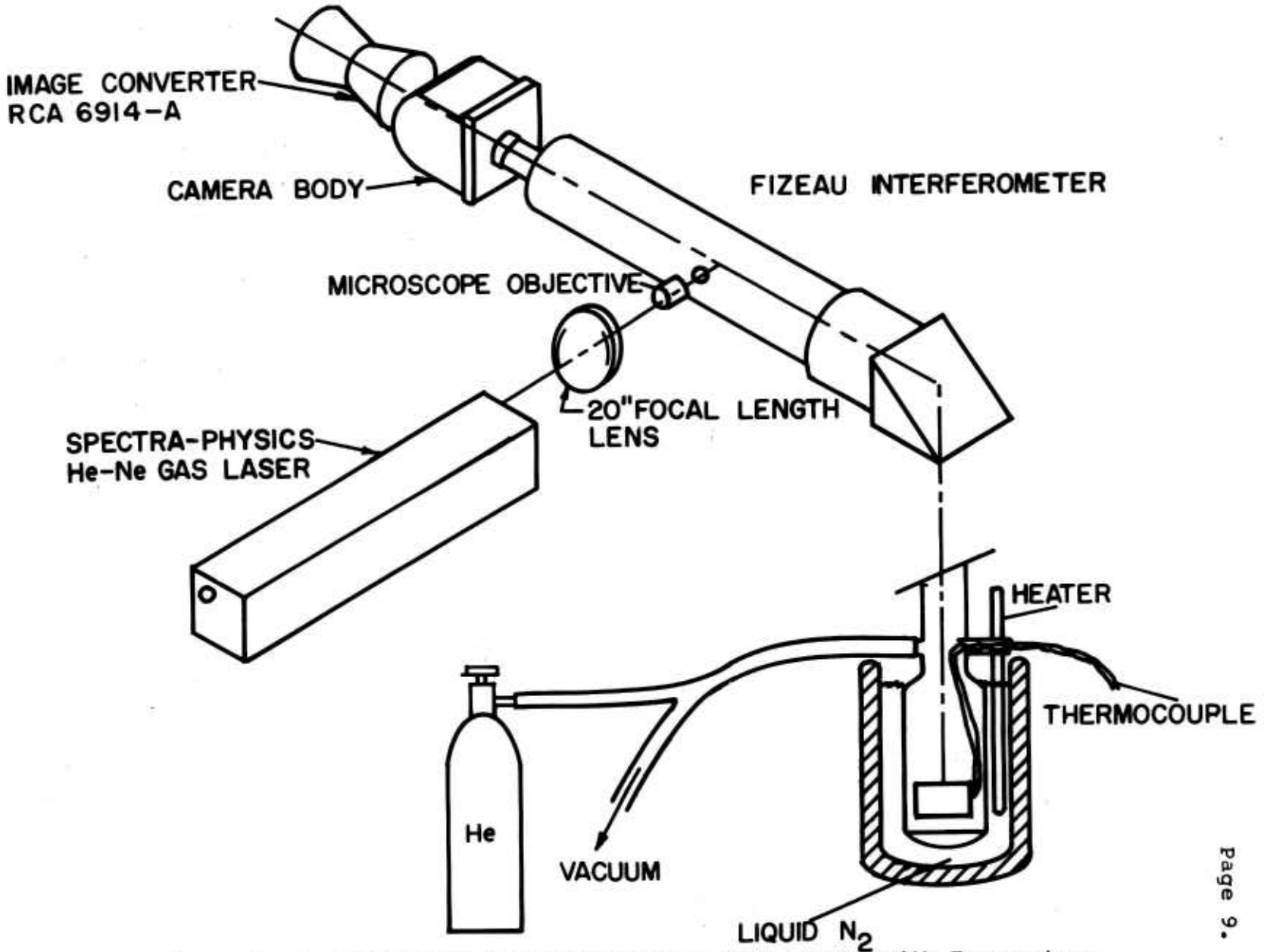

Figure 3. Apparatus for Measuring Optical Path Change with Temperature

frosting then placed in a dewar filled with liquid N_2. It was found necessary to admit helium to the sample container to facilitate cooling.

Each component of the apparatus has been tested individually and together at room temperature. Experiments will be made shortly to obtain data for various laser glasses from liquid N_2 to room temperature.

3. Particulate Inclusions in Glass

Platinum and other inclusions have been a problem in optical glass manufacture for may years. High quality optical glass is now manufactured nearly exclusively in platinum lined glass melting and fining tanks. The reason for this is that there is a smaller contamination problem, easier control over the process, greater volume, and better uniformily of the product. Until the advent of the glass laser, it had been unnecessary to decrease the inclusion level in the optical melting units below their present level.

The development of platinum lined optical melting units was undertaken to improve the quality, selection, etc. as mentioned above. The results justified the effort. There is no evidence that any other process of melting optical quality glasses will achieve the high quality standards set by our present melters.

We have initiated a Company sponsored inquiry into the causes and prevention of platinum "flake" in optical glass. This study will determine the factors and action required to minimize the incidence of inclusions which cause catastropic damage to lasers in platinum tank melted glass. At the same time recommendations are being drawn up to make major modifications in tank design, if they are required.

The greatest energy flux Code 0580 laser glass has been subjected is about 10^5 watts/cm^2 (4 millisec pulse). We have not found any destructive effects which may be interpreted as caused by an inclusion within the glass. However, only very large particles could be expected to absorb sufficient energy to destroy the laser as this energy level. We have been able to locate only a very few platinum inclusions in the 10 meters (1½" dia) of Code 0580 glass we have carefully examined. The remarkable freedom of Code 0580 glass from inclusions is most likely a consequence of the corrosion resistance of platinum to this type of glass (soda-lime silicate).

II. FLUORESCENCE OF GLASS FOR LASERS

1. Absorption of Long Fluorescence Lifetime Glasses

The measured Nd^{3+} fluorescence lifetime in glass is a function of the composition such as the amount and kind of network modifiers, e.g., Na, K, Rb and also the glass system, e.g. silicate, borate, phosphate.

The lifetime is determined by the degree of interaction of the f shell of the Nd^{3+} ion with its surrounding crystal field. This manifests itself as splitting of the free ion levels, appearance of vibronic transition, strength of the fluorescence and absorption, and the extent of non-radiative transitions from the metastable state.[3] The examination of the first two of these effects is difficult in glass due to the inherent broadness of absorption bands.[4]

Keeping this in mind one can compare the splittings of the low lying states of Nd^{3+} with predicted splittings according to the listed symmetry site. Table I shows this.

TABLE I

Crystal Field Splittings

	Free Ion Term Designation					
Site Symmetry	$^4F_{3/2}$	$^4I_{15/2}$	$^4I_{13/2}$	$^4I_{11/2}$	$^4I_{9/2}$	$^2G_{7/2}$ & $^2G_{5/2}$
Octahedral O_h Tetrahedral T_d	1	5	5	4	3	5
Icosahedral K	1	3	4	3	2	3
Hexagonal D_6 Trigonal D_3 Tetragonal D_4	2	8	7	6	5	7
Observed	2	4	2	2*	2*	5

*Determined from fluorescence

The data listed under "observed" is representative for Nd^{+3} in all glass looked at thus far. Very little can be concluded from this comparison except that the splitting of the $^4F_{3/2}$ state seems to indicate a symmetry of the Nd environment somewhat lower than that of cubic or icosahedral symmetry. However, other factors could account for the $^4F_{3/2}$ splitting, e.g., a dynamical Jahn - Teller effect. Previous work done by Stevens[5] and Judd[6] on the crystal field computation of rare earth ions in crystal (ethyl sulfates, double nitrates and the trichlorides) have used the model of the Nd^{+3} ion surrounded by nine nearest neighbors arranged so that the site symmetry is C_{3h}.

A point of interest is the four bands involved in the $^4F_{9/2}$ - $^4I_{15/2}$ transitions. There is a relatively strong band at 6321 cm^{-1} and three weaker ones on the long wavelengths side at 5912, 5822 and 5777 $cm.^{-1}$ respectively. The spacing of the three weaker lines from the strong line, at 6321 cm^{-1} are 409, 499, 544 $cm.^{-1}$ respectively, corresponds to a region of strong absorption due to the glass lattice[7] (see Fig. 4). It was first thought that these bands might be due to electronic-vibration interactions. If this were the case, however, one would expect that these bands would show up on the high energy side of the pure electronic transition especially at liquid N_2 temperature. This was not observed, so the four bands are taken as crystal field splittings of the $^4F_{15/2}$ state.

In general the absorption spectra of Nd^{+3} glasses look the same as far as position and number of absorption bands are concerned. However, there are a few distinguishing features from one glass system to another. Figure 5 shows the 5800 Å absorption band region for a Rb, K, and Na silicate glass and also a borate and tellurite glass. The Rb and K glasses, which have long fluorescent lifetime ($\sim$1 msec.), have a sharper spectrum than the corresponding shorter lifetime glass represented here by a Na silicate glass - i.e., the individual bands seem to be somewhat more resolved. The borate and tellurite glass, also glass containing Al_2O_3 are characterized by a diffuse spectrum as is shown in Fig. 5 for the 5800 Å line. These glasses all have characteristically very short fluorescent lifetimes. The major difference betweeen the Rb and K glass spectra and the Na spectrum is the change of the relative heights of the 5840 Å band of the relative heights of the 5840 Å and 5700 Å lines -- i.e., the ratio of these

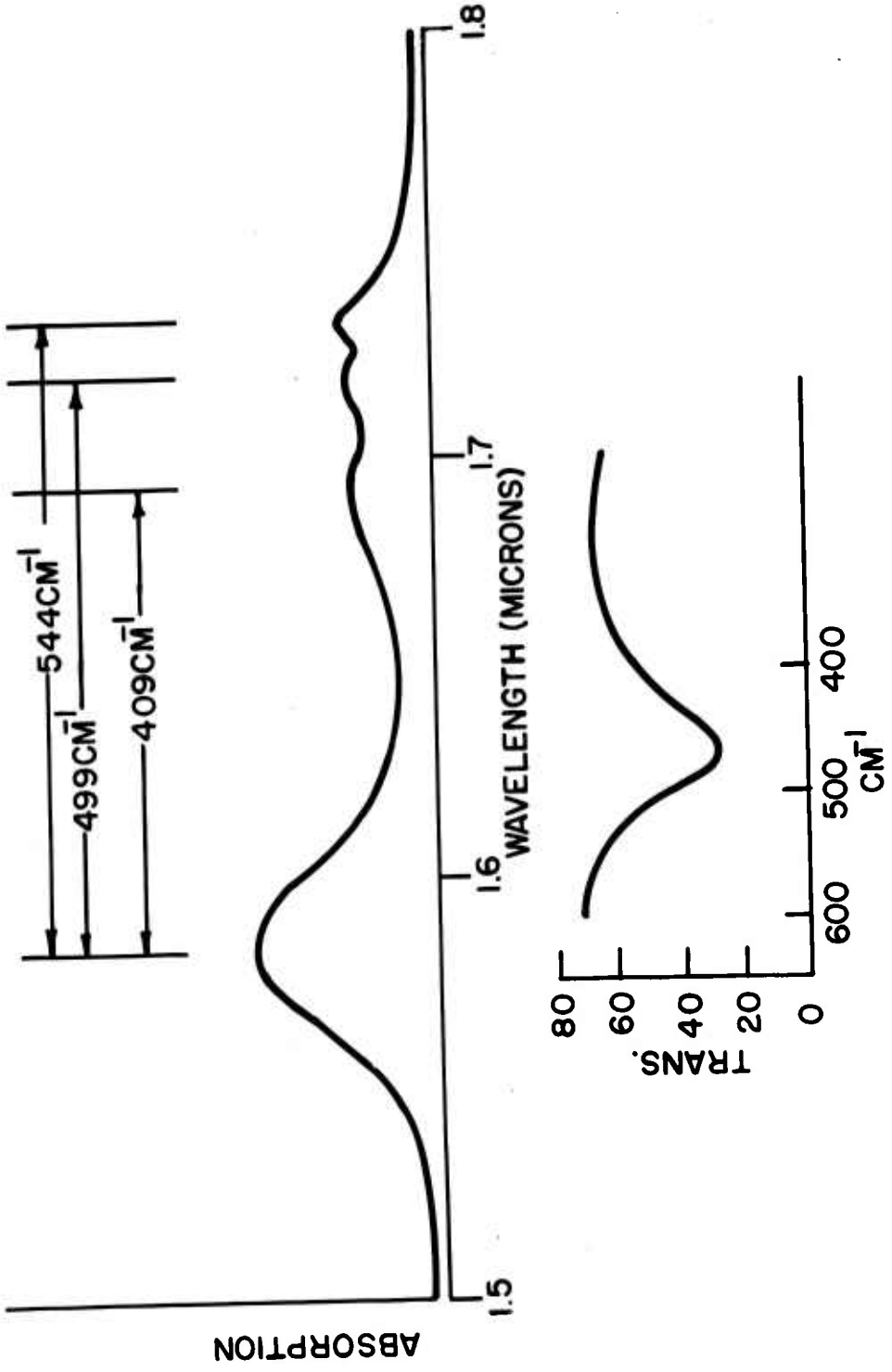

Figure 4. Absorption of Rubidium Silicate Glass at 1 N_2 Temperature

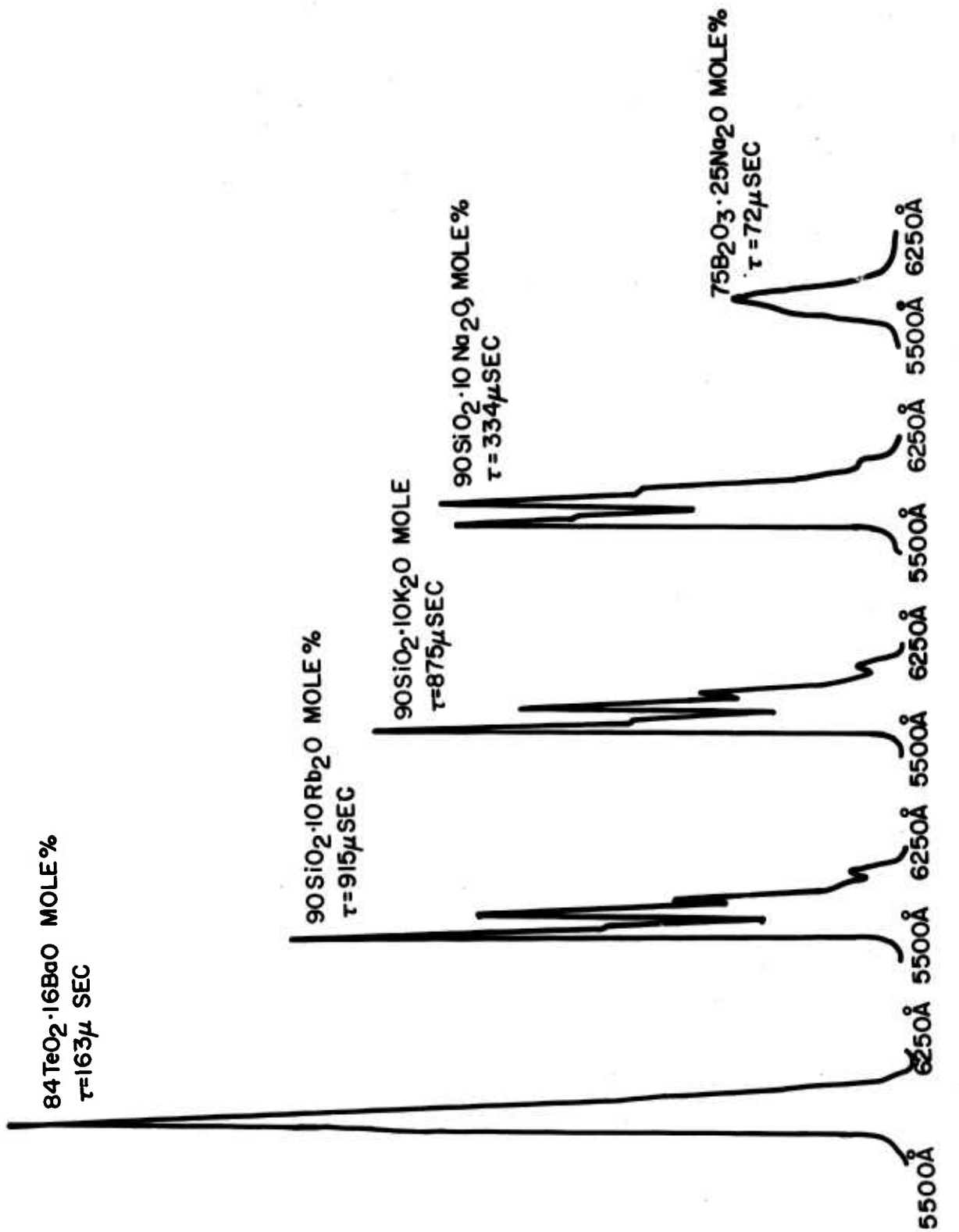

Figure 5. 5800Å Absorption Band of a Series of Glasses

heights inverts when passing from Na to Rb and K. In silicate glasses it seems that this absorption characteristic is always present when the heavy alkali ions are present. However, in a Cs_2O-B_2O_3 glass the 5800 Å band is broad and has a short lifetime typical of the sodium borates. In a germanate glass which has a composition of 75 GeO_2·10 BaO·15 K_2O the 5800 Å line does not show this effect even though K_2O is present and indeed the lifetime is relatively short. Figure 6 shows the comparison of this germanate glass with its silicate analog - i.e., 75 SiO_2·10 BaO·15 K_2O. So it seems that this effect, i.e., $\alpha 5700 > \alpha 5840$, does indicate a long lifetime, however, just how this is brought about is not known as yet.

2. Relative Quantum Efficiencies and Transition Probabilities of Long Lifetime Glasses

As stated before, the lifetime is a function of the kind and concentration of network modifiers. Figure 7 shows for example a graph of τ vs. mole % Cs_2O at two concentrations of Nd^{3+} and τ vs. mole % K_2O. The lifetime is determined by two factors, 1) the quantum efficiency and, 2) the $^4F_{3/2} - {}^4I_{11/2}$ transition probability. In order to get some idea of the relative values of these two quantities one can define a relative quantum efficiency by the expression.

$$\phi_{eff} = \frac{\text{Area under } 1.06\mu \text{ emmission line}}{\text{Area under absorption spectrum from } 3000 - 9000 \text{ Å}}$$

This factor was determined for a number of glasses where the area under the fluoresence line was determined by an intensity measurement using wide slits and thus effectively integrating the output. The area under the absorption curve was determined by a planimeter measure-

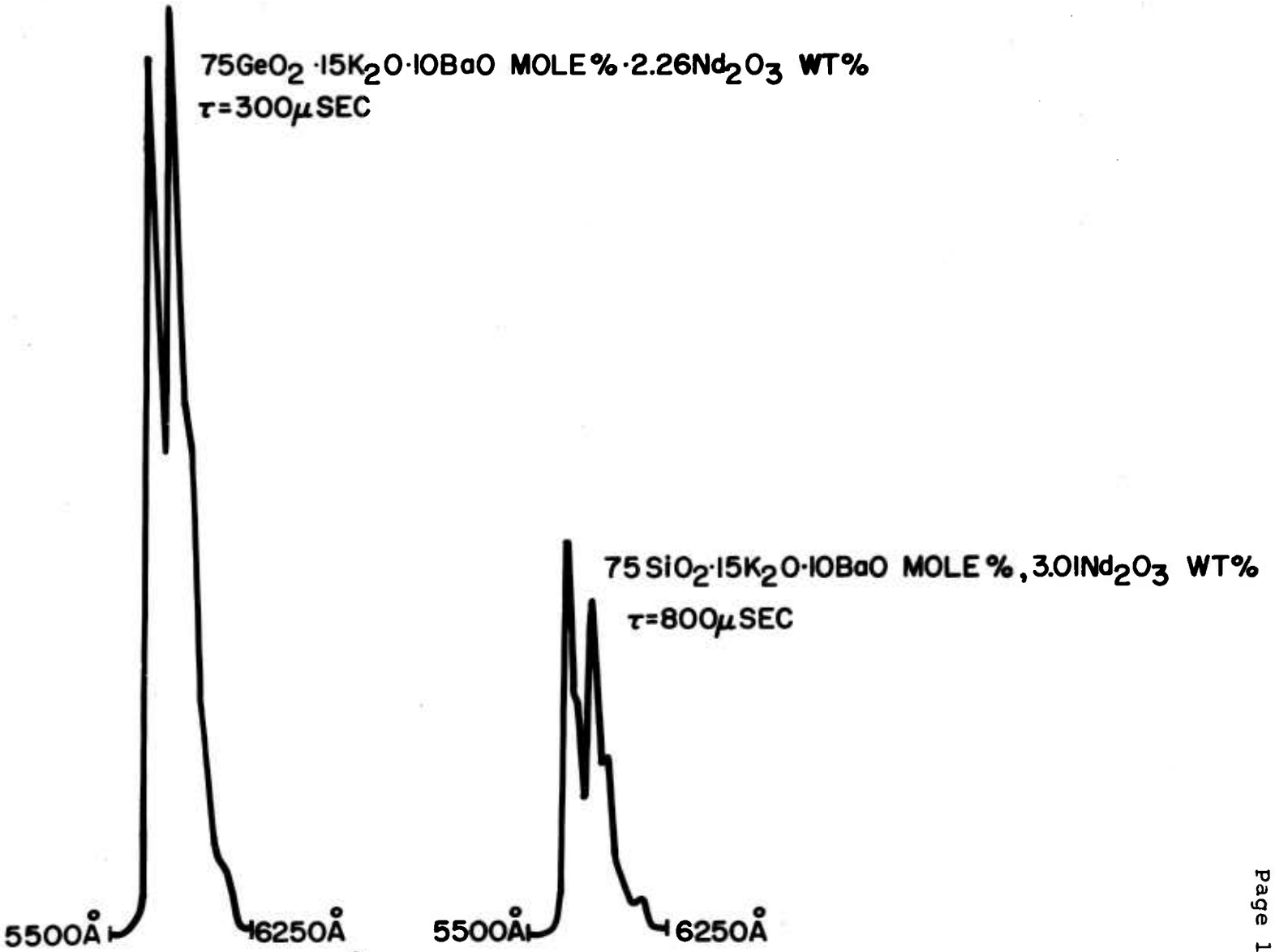

Figure 6. 5800Å Absorption Band of a Germanate and a Silicate Glass

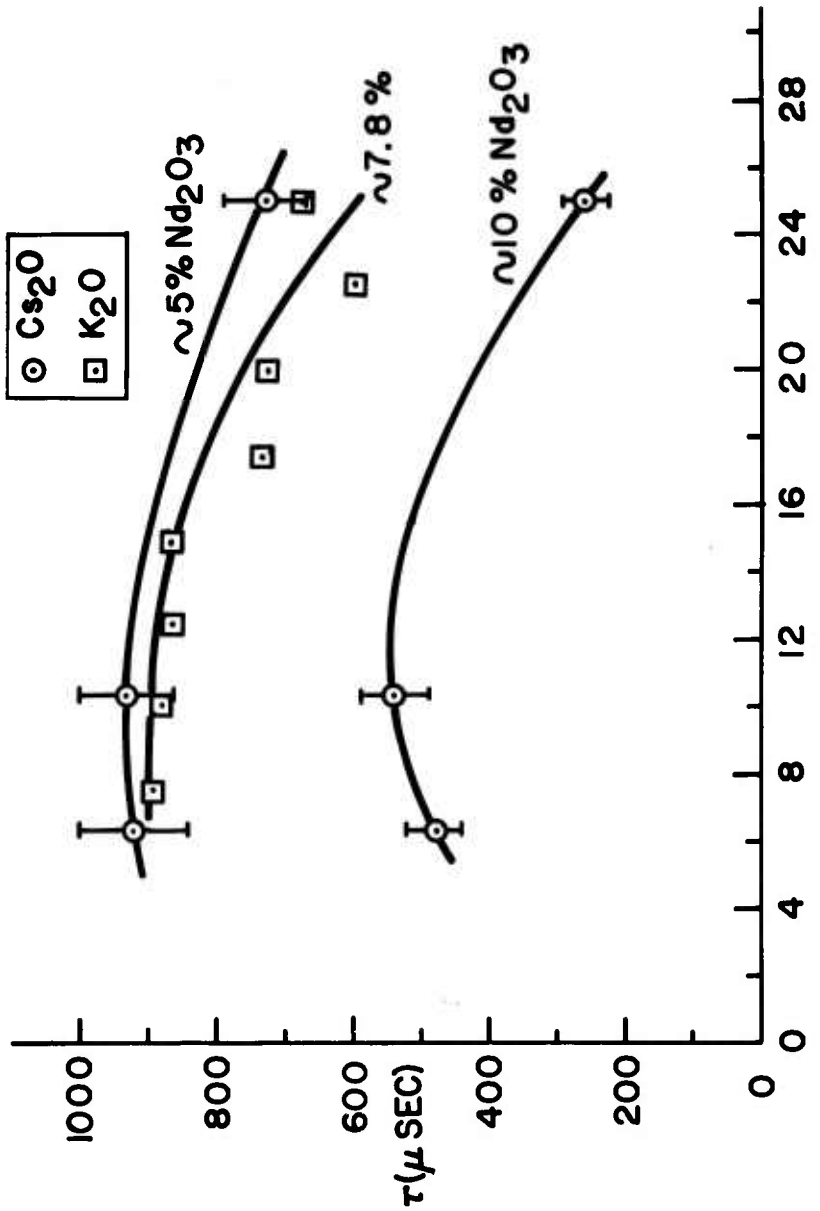

Figure 7. Lifetime vs Mole % Cs_2O and K_2O in a $90SiO_2 \cdot 10R_2O$ Glass

ment of the absorption curve of a 1 mm sample from 3000 to 9000 Å. Table II lists these glasses where KA is defined as the relative transition probability computed as

$$KA_{1.06\mu} = \frac{\Phi_{eff}}{\tau_m}$$

The reliability of the ϕ_{eff} is estimated to be about 10-15% while that of KA is about 20-25%. Figure 8 shows the variation of ϕ_{eff} and KA with Nd^{3+} ions/cc in a Rb, Na and K silicate glasses of comp. 90 SiO_2· 10 M_2O. The ϕ_{eff} falls off more sharply in the order Na K Rb. The same result is obtained for the relative transition probability. Figure 9 shows the same data in a different way where we have plotted the ϕ_{eff}, and KA vs. the ionic radius of the modifier cation for two different Nd^{3+} concentrations. The ϕ_{eff} at 1.7×10^{20} ions/cc data can be loosely interpreted as remaining relatively constant within the accuracy of these measurements ($\sim$ 10-15%). At the higher Nd^{3+} concentration the faster rate of concentration quenching of the Na ion comes in and the quantum efficiency increases from Na to K to Rb. The KA seems to behave more orderly and decreases roughly linearly with increased ionic size. The absorption cross section of the 8800 Å ($^4F_{9/2} - {}^4F_{3/2}$) band is plotted vs. the cation size and gives a linear relation decreasing with increase in size.

Of interest also in Table II is the high transition probability of the phosphate and tellurite glasses and also the difference in quantum efficiency of the Ba-K-SiO_2 and Ba-K-GeO_2 glasses. These two glasses were mentioned above with respect to large differences in lifetime, here it seems this is entirely due to quenching since the transition probability is constant within the accuracy of the data (about 20%).

TABLE II

Computed Quantum Efficiencies and Transition Probabilities

Molor Comp.	Nd^{3+} ions/cc	τ meas. μsec.	ϕ_{eff}	KA
$90SiO_2 - 10Cs_2O$	1.86	1000	2.16	.22
$90SiO_2 - 10Rb_2O$	1.81	1034	2.60	.25
$90SiO_2 - 10Rb_2O$	4.5	915	2.18	.24
$90SiO_2 - 10Rb_2O$	8.9	780	1.39	.18
$90SiO_2 - 10K_2O$	4.1	900	2.12	.24
$90SiO_2 - 10Na_2O$	4.1	334	1.15	.35
$90SiO_2 - 10Na_2O$	8.0	182	.37	.20
Rb - Ba Crown	1.8	970	2.9	.30
Rb - Ba Crown	6.83	790	1.39	.17
Soda-lime silicate	4.4	340	1.41	.42
$75B_2O_3 - 25Na_2O$	1.48	71	.27	.39
$84TeO_2 - 16BaO$	2.86	164	1.06	.65
$75SiO_2$-$15K_2O$-10BaO	2.99	805	2.47	.31
$75GeO_2$-$15K_2O$-10BaO	2.99	805	2.47	.31
$90SiO_2 - 10K_2O$	1.67	964	2.94	.31
$90SiO_2 - 10NaO_2$	1.66	580	2.90	.50
$78P_2O_5 - 22La_2O_3$	0.91	311	1.93	.62

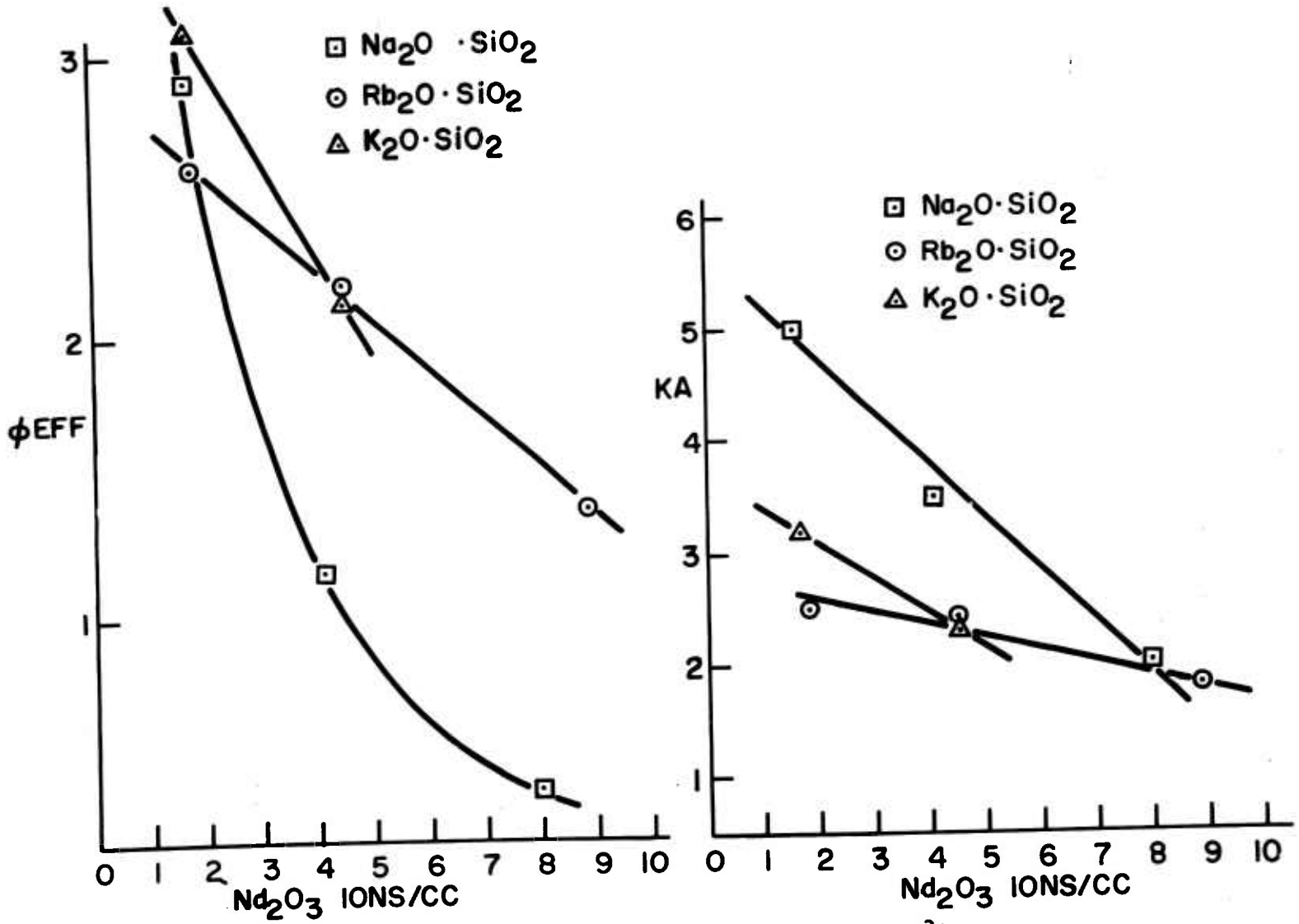

Figure 8. a) Quantum Efficiency vs Nd^{3+} ions/cc
b) Transition Probability vs Nd^{3+} ions/cc

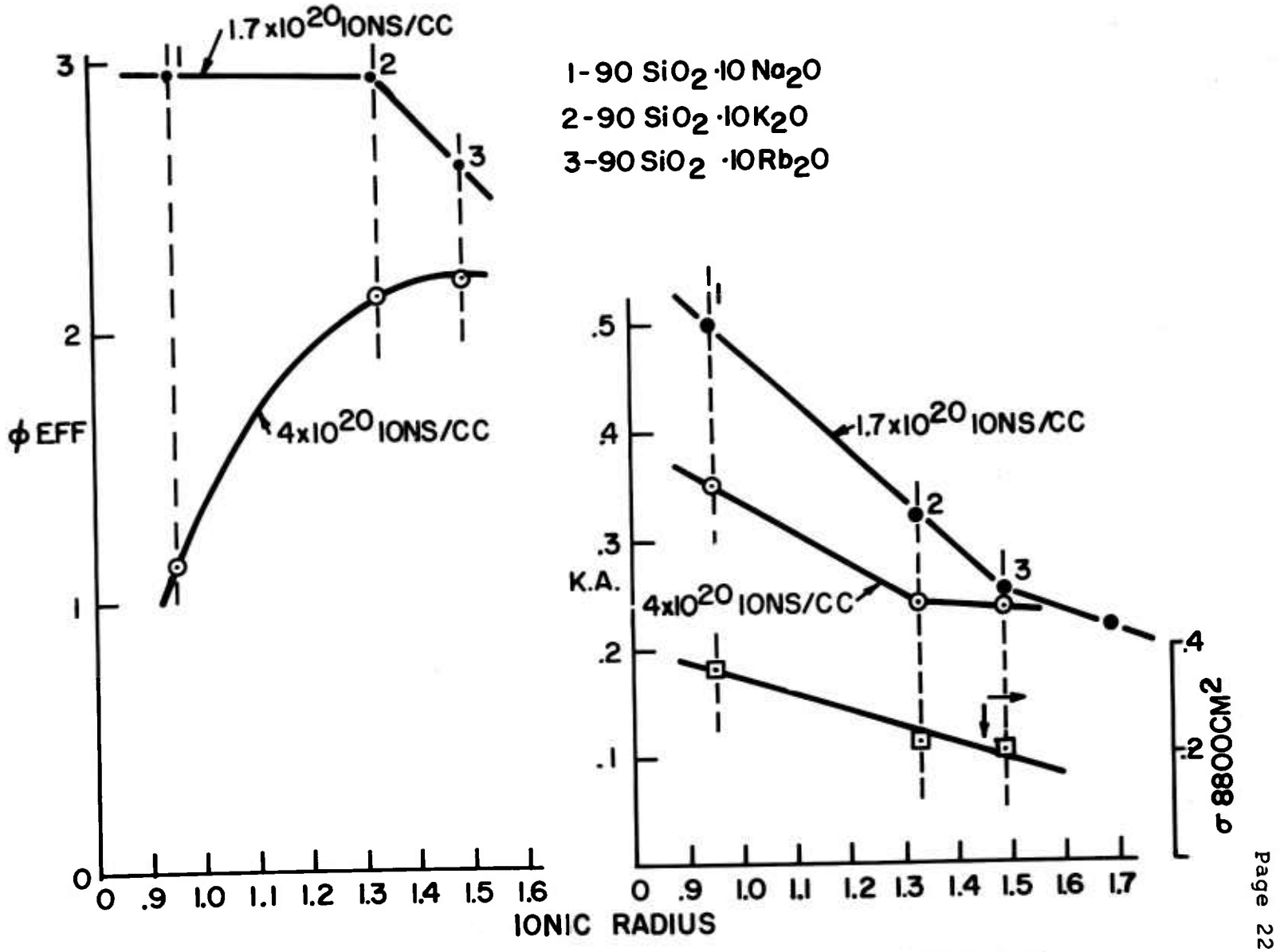

Figure 9. Computed Properties vs Ionic Size of Modifier Cation

A correlation was made of τv^3 vs, oxygen ions.[7] The idea was, briefly, that the oxygen ions per unit volume were a measure of the interaction of the lattice with the Nd^{3+} ion. The τv^3 is the lifetime normalized to the index of refraction.[1] Figure 10 shows the results for the glasses measured recently and the dotted line is the correlation obtained with a previous set of glasses.[8] The glasses with a high Nd^{3+} content are denoted by x's since here the concentration quenching effect is more important. If one excluded these points it is interesting to note that the data almost all falls above the dotted line.

3. General Conclusions

What has been seen thus far is that certain modifying cations increase the fluorescence lifetime in a somewhat orderly fashion and in general this can be shown to be due to an increase in quantum efficiency and/or a decrease in the transition probability. From the absorption and fluorescence data it appears that, save for the sharpening of the absorption spectra and the relative heights of the two 5800 Å bands, the number of lines and their spectral positions vary little from glass to glass. (The increased sharpness of the absorption spectra of the longer lifetime glasses may indicate a somewhat more ordered arrangement of the Nd^{+3}). This can be interpreted as meaning that the same average crystal field environment i.e. symmetry, coordination, is seen by the Nd^{+3} in the various glass compositions that have been studied thus far. Yet, within this, the transition probability of certain transitions, primarily those in the infrared, can vary by as much as a factor of four.

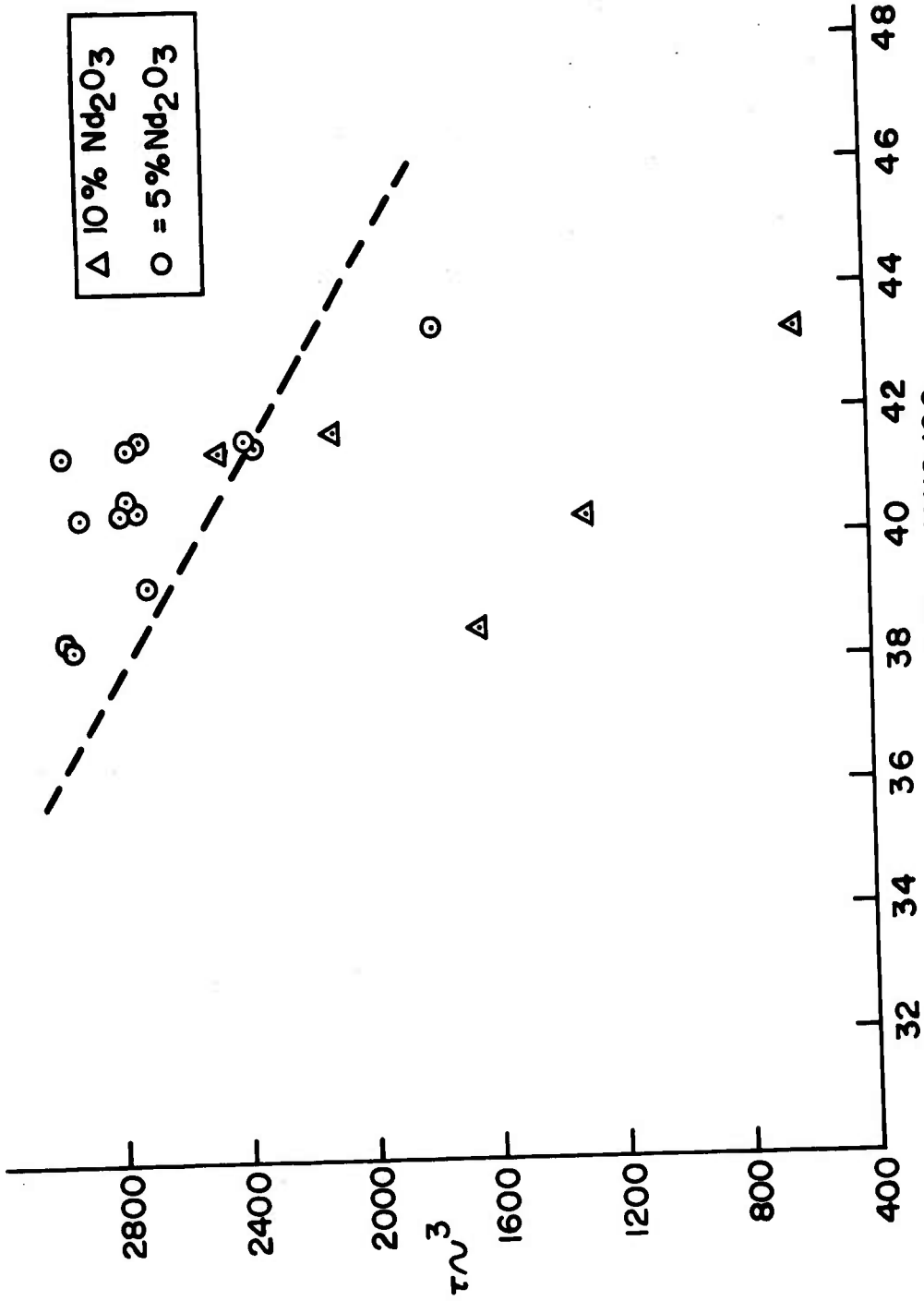

Figure 10. Lifetime (Refractive Index)^3 vs Oxygen ions/cc

Judd[9] states that for most of the rare earth ions in crystals, the lines usually appear to fall in groups which, as a whole, are constant for various salts of a particular rare earth ion. The structure as well as the intensity and number of lines of the group vary considerably from salt to salt. This he ascribes to the effect of different crystal fields acting on the rare earth ion. As we discussed above, the disorder of the glass matrix would tend to mask the difference in structure and number of lines within a given group as described by Judd. What one would expect then is exactly what one sees, viz, the constancy of the general spectral position of the groups from glass to glass (which can be thought of then as crystal to crystal) and the only variation that would be seen is the intensity of the group as a whole which would not be masked by the general diffuseness of the spectrum.

It is likely that the Nd^{+3} has the same coordination in most oxide glasses since this is defined primarily by the charge and size of the Nd^{+3} itself and oxygens which surround it, however, this arrangement can give rise to different crystal field potentials which are usually expressed as

$$V_{crs} = \sum A_n^m V_n^m$$

where V_n^m are potential functions which transform like the corresponding spherical harmonics Y_n^m and the constants A_n^m which depend upon the lattice. Thus even under the same symmetry the V_n^m would necessarily be the same but the A_n^m would differ. Van Vleck has shown[10] that the transition probability is given approximately by

$$A = A_{allowed}(V_{hem}/h\nu)$$

where

$$V_{hem} = \langle \Psi^{\circ}(4f) \left| V_{crs} \right| \Psi^{\circ}(5d) \rangle$$

$$h\nu' = E_{5d} - E_{4f}$$

Thus for the same symmetry of Nd^{3+} in, for example, a Na and a Rb silicate glass we could say that (V_{crs}) Na > (V_{crs}) Rb. That is, the perturbation term is smaller for a Rb glass than with a Na glass. Exactly why this is so is still to be discovered.

4. Measured Thresholds versus Thresholds Calculated from Fluorescence

In principle, the oscillation threshold of a glass laser can be calculated from its measured fluorescent properties.[8] Attempts to check this calculation with experiment met with limited success. A possible source of the discrepancy could be the variation of internal loss from one laser to another since the calculation assumed equivalent losses. A correction for this variation has been made.

The loss was measured for a series of laser rods, ¼" dia, by 2" long, by the method described previously.[1] The thresholds were measured in an arrangement consisting of two FX-38A flash tubes strapped by silver foil to a PYREX® brand tube into which the laser was placed. Table 3 shows the pertinent data.

TABLE III

Glass	Meas. Threshold Joules	Loss %/cm.	Calc. Threshold
CIN	48	0.79	0.88
CIK	35	1.25	1.09
CEM #5	32	0.70	0.88
CEH	>700 *	3.63	4.30
CJF	30	0.75	0.50
CJF #16	75	0.76	0.50
DGN	65	0.98	0.61
CJI	>800 *	7.66	15.20
CEH #26	400 *	3.29	4.70
CIK	40	1.31	1.14
CIL	>700 *	12.40	8.10
CDP	>700 *	0.76	1.10
DGM #28	77	0.83	0.37
DGL #2	40	1.06	0.42
CEN #20	39	0.53	0.66
0580	13 **	0.50	0.21

*400μf

** 20μf

The correlation is shown in Fig. 11. The agreement is poor. However, a consoling feature, which is of importance, is that the absorption loss measurements are qualitatively verified. (Refer to Table III) Rods with losses ca. 1.5%/cm would not go with pumping energies up to 160 J and losses ca. 3.5%/cm would not go for energies up to 700 J.

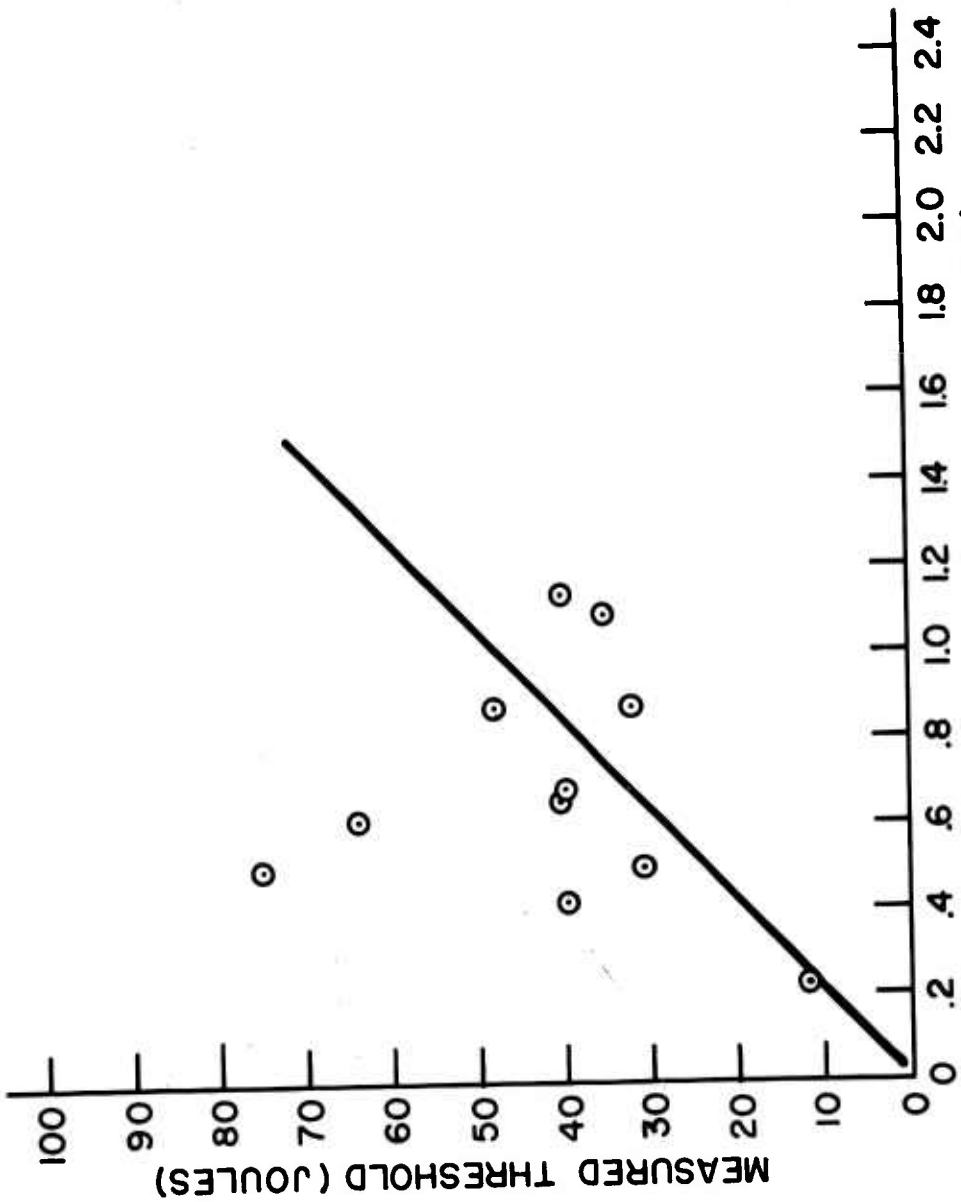

Figure 11. Calculated vs Measured Threshold

III. THEORY OF ENERGY DISTRIBUTION IN A Nd^{3+} DOPED GLASS LASER ROD

1. Introduction

The input energy to an optically pumped laser is absorbed on traversing the diameter of the rod with part of the energy used to attain inversion and part going into heating. A quantitative knowledge of this absorption is important for determining, 1) the gain across the rod diameter, and 2) the degree of unequal heating which causes optical distortion. Sooy & Stitch[11] have calculated the energy density distribution in a rod immersed in a spatially homogeneous radiation field. Numerical values appropriate to ruby characterized the focusing effect. A single absorption coefficient was assumed for the rod.

A simple experiment measuring the fluorescence in a slab as a function of depth showed that a single absorption coefficient could not be used to characterize the pumping. In this paper we extend the analysis in terms of an absorbed energy density which includes the wavelength dependence of the pump light and the optical absorption of the rod. Numerical values are calculated for a neodymium containing glass excited with a xenon source.

2. Absorbed Energy Distribution in a Slab

In order to determine the effect of the wavelength dependence of the aborption the following experiment was performed. The fluorescence intensity from a 1 mm slit as a function of depth was measured on a slab of glass containing a Nd^{3+} concentration of 4.4×10^{20} ions/cc. (Fig. 12). The experimental data shows that a single expontential attenuation cannot be used. This can be seen by considering the non-constantcy of the ratio of any two consecutive points. Even if it is desired to approximate this

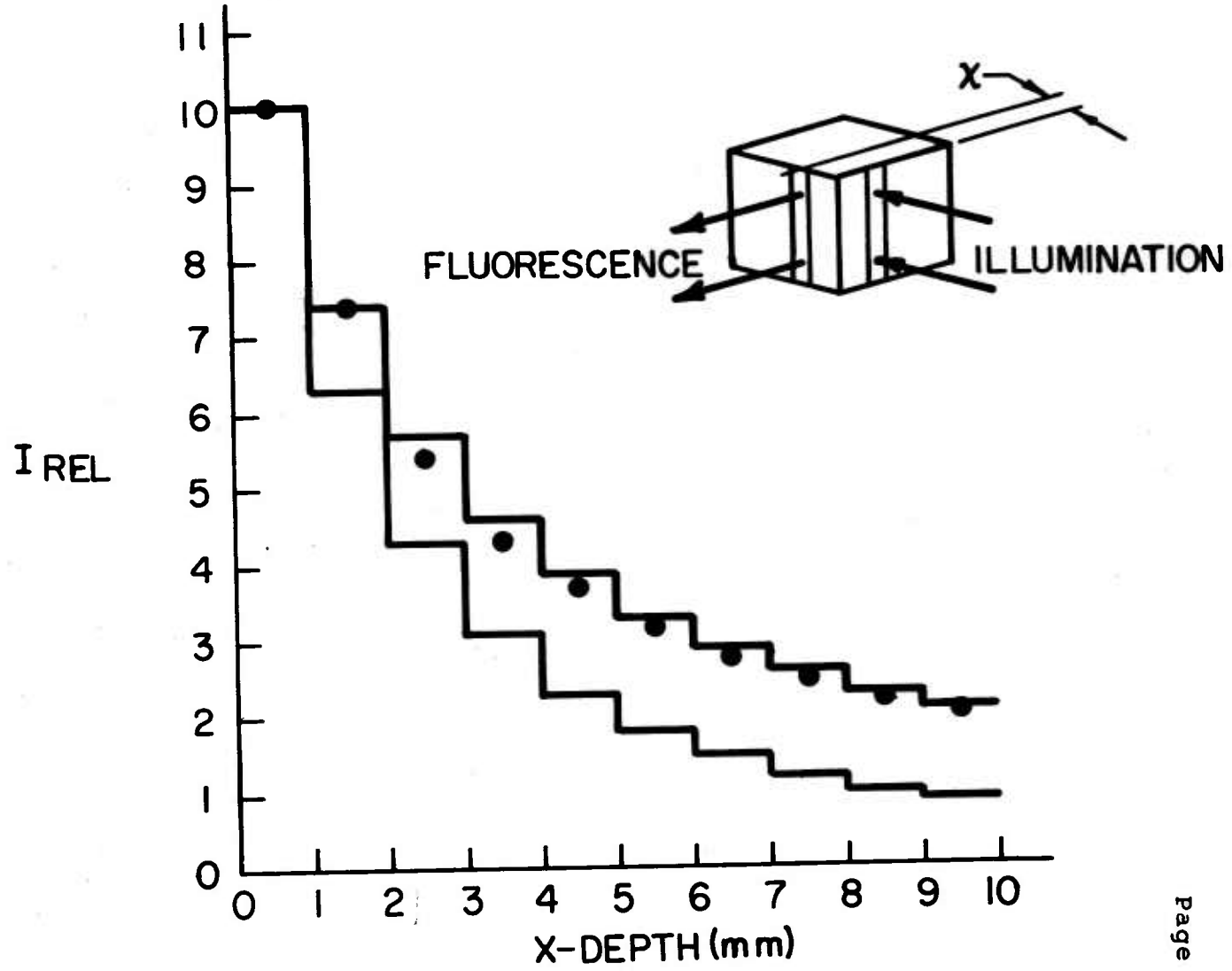

Figure 12. Relative Fluorescence Intensity from a 1mm Slit as a Function of Depth in Code 0580 Glass

data by a single expontential there is no a priori way to arrive at its numerical value.

The equations appropriate for the absorption are given as follows:

(1)... $$F \propto I_{abs} = \int_{\Delta x} \int_{\nu} I(\nu, \chi) \alpha(\nu) \, d\nu \, d\chi$$

since $$I(\nu) = I_0 \exp[-\alpha(\nu)\chi]$$

then $$F(\Delta\chi) \propto \int_{\nu} e^{-\alpha\chi}(1 - e^{-\alpha\Delta\chi}) \, d\nu$$

where

F = fluorescence intensity

I = energy absorbed

α = absorption coeff.

χ = depth

Rigorously, the integrand on the right hand side of equations 1 and 2 should be divided by $h\nu$ to obtain the quantum equivalence between absorbed energy and excited atoms. This was neglected since the variation of absorption coefficient with the wavelength is similar in all regions of the spectrum. Making use of the absorption spectrum of Code 0580 glass, we computed the integral on the right of equation 2 for two cases. The first case makes use of a delta function dependence of α on frequency, that is ignoring all contributions other than from the absorption spectra maxima. The integral reduces to just the sum of the integrands for each absorption peak. The second case was to integrate equation 2 over the wavelength regions 3000 - 9000 Å. This was accomplished by machine computation taking 50Å intervals of wavelength. Figure 12 shows the computed results for the two cases and also the experimental data. The

computed data was normalized to the first experimental point of the sample. The agreement between the integrated case and the experimental data is very good indicating the importance of taking into account the contribution from the entire spectrum.

3. Absorbed Energy Distribution in a Rod

The expression for the normalized energy density at a point χ written in reduced variables (Fig.13) according to Sooy & Stitch[11] is:

$$(3)\ldots \quad \epsilon(\chi)=\frac{n^3}{4\pi}\int_{\phi}\int_{-\zeta}^{\zeta}\frac{T(\beta)\exp[-\alpha R\rho](1-\chi\cos\phi)}{\rho^3}\,d\zeta\,d\phi$$

where

$$(4)\ldots \quad T(\beta)=1-\left\{\frac{\cos^2\beta(1-n^2\sin^2\beta)+n^2\sin^4\beta}{[\cos\beta(1-n^2\sin^2\beta)^{1/2}+n\sin^2\beta]^2}\left[\frac{(1-n^2\sin^2\beta)^{1/2}-n\cos\beta}{(1-n^2\sin^2\beta)^{1/2}+n\cos\beta}\right]^2\right\}$$

$$(5)\ldots \quad \frac{\rho}{R}=(1+\zeta^2+\chi^2-2\chi\cos\phi)^{1/2}$$

the limits are:

$$(6)\ldots \quad \chi\le\frac{1}{n} \qquad 0\le\phi\le 2\pi$$

$$\chi>\frac{1}{n} \qquad -\phi_1\le\phi\le\phi_1\ ,\ -\phi_2\le\phi\le\phi_2$$

$$(7)\ldots \quad \begin{Bmatrix}\phi_1\\ \phi_2\end{Bmatrix}=\sin^{-1}\left[\frac{(n^2-1)^{1/2}}{n^2\chi}\begin{Bmatrix}-\\ +\end{Bmatrix}\frac{(n^2-\frac{1}{\chi^2})^{1/2}}{n^2}\right]^{1/2}$$

$$(8)\ldots \quad \zeta=\pm\left[\frac{1-2\chi\cos\phi}{n^2-1}+\frac{\chi^2\cos^2\phi\,n^2}{n^2-1}-\chi^2\right]^{1/2}$$

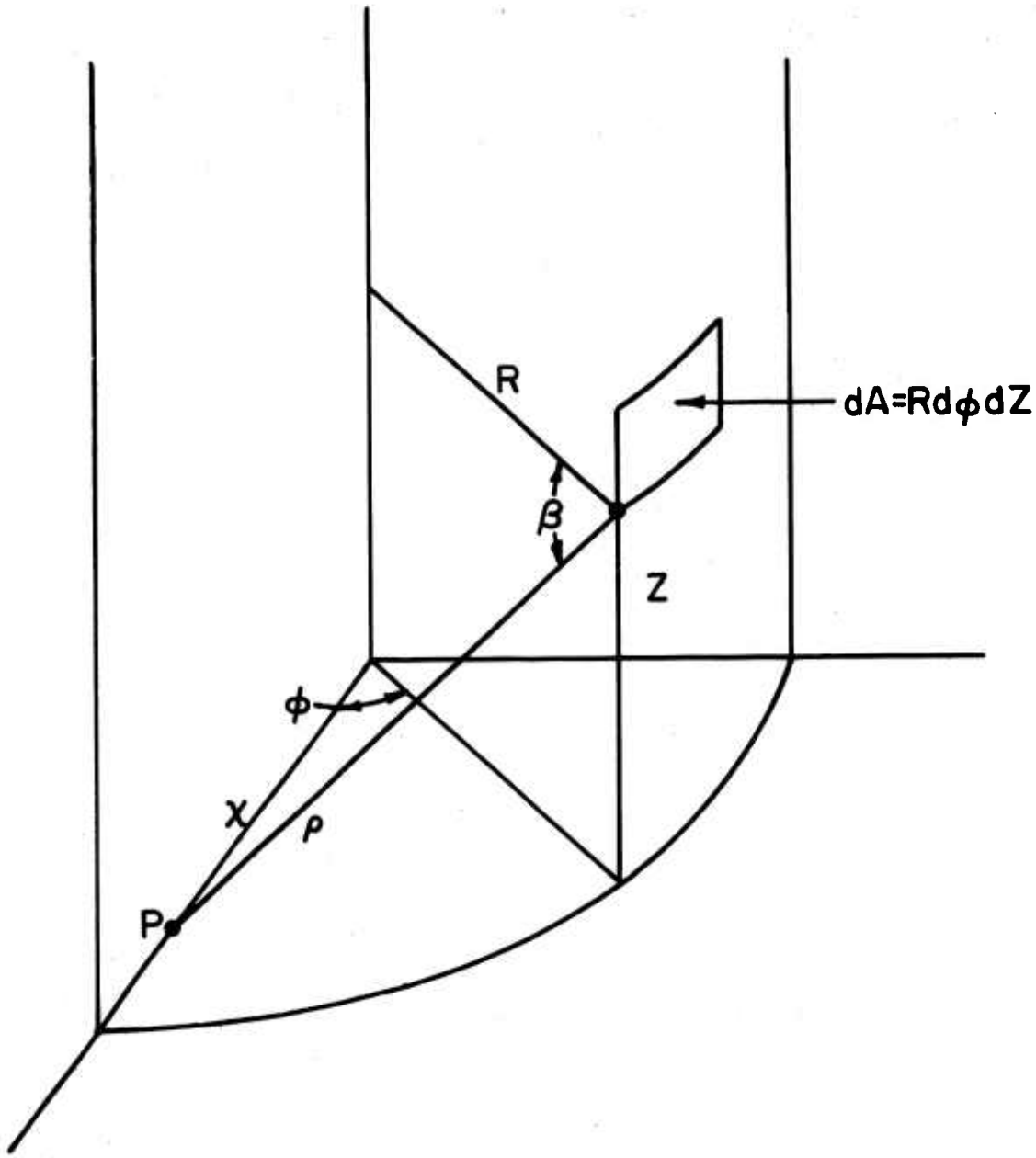

Figure 13. Coordinate System Used in the Energy Density Calculation

The effect of reflection back in to the rod after one pass was ignored which is important only for small values of αR.

The monochromatic energy density distribution does not give a complete description since one is concerned with absorption coefficients and energy sources which are frequency dependent. In order to take this into account, one can compute the energy absorbed per interval of radius which is given by

$$(9)\ldots \quad \epsilon_{abs}(\Delta\chi) = \frac{1}{\Delta\nu}\int_{\nu}\int_{\chi}\alpha(\nu)\,\epsilon(\nu,\chi)\,P(\nu)\,d\chi\,d\nu$$

where

$\alpha(\nu)$ is the absorption coefficient

$\epsilon(\nu,\chi)$ is the energy density

$P(\nu)$ is the pump spectrum

This integral is over the entire pump spectrum and therefore the contribution from weak absorption bands as well as the wings of strong bands are taken into account. These contributions account for nearly all the pumping near the center of the rod at high Nd^{3+} concentrations. In order to evaluate equations 9, the first step is to compute the monochromatic energy density as a function of the reduced radius χ according to equation (3) for a number of αR's for a Nd^{3+} glass composition (in this case Code 0580 glass see Table IV and Figure 14). In order to check the accuracy of the computation, the energy density at several values of χ was calculated for ruby and compared to the results obtained by Sooy & Stitch.[11] The agreement was within 1 percent for each of these points. With this data, the absorption

TABLE IV

Energy Density as a Function of χ & α_R for Code 0580 Glass

0	.05	.15	.25	.35	.45	.55	.65	.75	.85	.95
α_R=0	2.151	2.137	2.104	2.0532	1.961	1.7875	1.425	1.1156	.9385	.80
.05	2.054	2.043	2.011	1.953	1.865	1.704	1.361	1.065	.902	.765
.707	1.994	1.986	1.963	1.911	1.818	1.668	1.329	1.039	.883	.750
.1	1.946	1.936	1.907	1.855	1.768	1.624	1.295	1.013	.862	.715
.1414	1.865	1.852	1.825	1.776	1.689	1.556	1.250	.975	.831	.700
.2	1.747	1.739	1.718	1.673	1.592	1.469	1.184	.922	.785	.669
.283	1.594	1.587	1.568	1.530	1.468	1.359	1.101	.863	.744	.620
.4	1.407	1.404	1.392	1.384	1.314	1.223	.994	.780	.671	.57377
.566	1.1895	1.168	1.157	1.1425	1.118	1.060	.864	.685	.604	.514
.8	.915	.918	.919	.916	.900	.861	.721	.584	.524	.463
1.13	.632	.641	.660	.676	.678	.658	.584	.488	.439	.414
1.6	.389	.396	.405	.424	.450	.463	.426	.389	.379	.37741
2.26	.201	.205	.215	.234	.265	.287	.292	.303	.324	.349
3.2	.072	.076	.086	.012	.136	.165	.176	.222	.262	.328
4.52	.015	.020	.025	.032	.050	.090	.114	.149	.204	.301
6.4	.002	.002	.003	.009	.015	.027	.049	.086	.152	.27291
9.04	.000	.000	.000	.000	.000	.004	.020	.042	.092	.233
12.8	.000	.000	.000	.000	.000	.000	.003	.014	.052	.190
18.80	.000	.000	.000	.000	.000	.000	.000	.003	.033	.142
25.6	.000	.000	.000	.000	.000	.000	.000	.000	.016	.0927

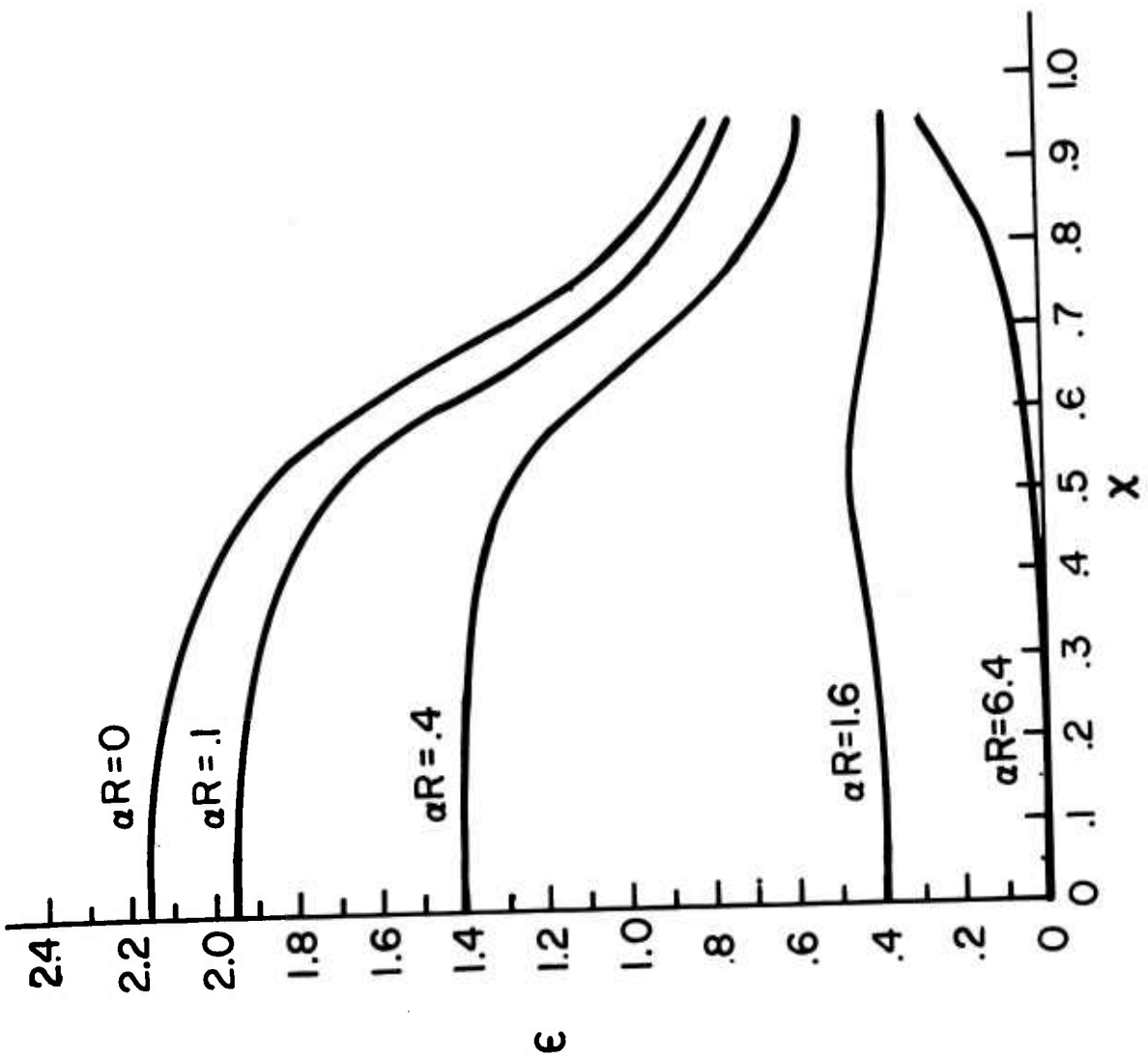

Figure 14. Monochromatic Energy Density vs Normalized Radius for Code 0580 Glass

spectrum, and the pump spectrum, we can integrate equation (8) over χ intervals. This was done with the following approximation.

$$\int_{\chi_1}^{\chi_2} \epsilon \, d\chi \approx \bar{\epsilon} \Big|_{\frac{\Delta\chi}{2}} \Delta\chi$$

This approximation was used since a fine set of ϵ vs χ data which is needed to integrate over χ involves considerable machine time and it was decided that in small χ intervals the approximation would be satisfactory.* Figure 15 and Table V show the results as the normalized absorbed energy in an interval $\Delta\chi = 0.1$, with ρR as the parameter where ρ is the Nd^{3+} concentration in ions/cc and R is the radius of the rod in cm.

4. Discussion

The qualitative aspects of Figure 15 can be derived from the monochromatic energy density data (Figure 14). In Figure 16 $\epsilon \alpha R$ vs. χ is plotted for low (0.05), medium (1.6), and high (12.8) values of αR. The integral of equation 8 is made up of $\epsilon \alpha R$ terms of the type given in Figure 16. αR and ρR are related by

$$\alpha R = \sigma \rho R$$

where σ is the absorption cross section.

At low αR values the contributions to the absorbed energy density are comprised of terms of small αR's and intermediate αR's, since most of the absorption cross sections are less than 1.5×10^{-20}. The shape of the energy absorbed curve vs χ will be approximated by the sum of the small αR curve and the intermediate αR curve of Figure 16

*The shape of the Xenon pump spectrum was measured from 5000 to 9000Å and for 3000 to 5000Å the shape was taken from information supplied by General Electric.

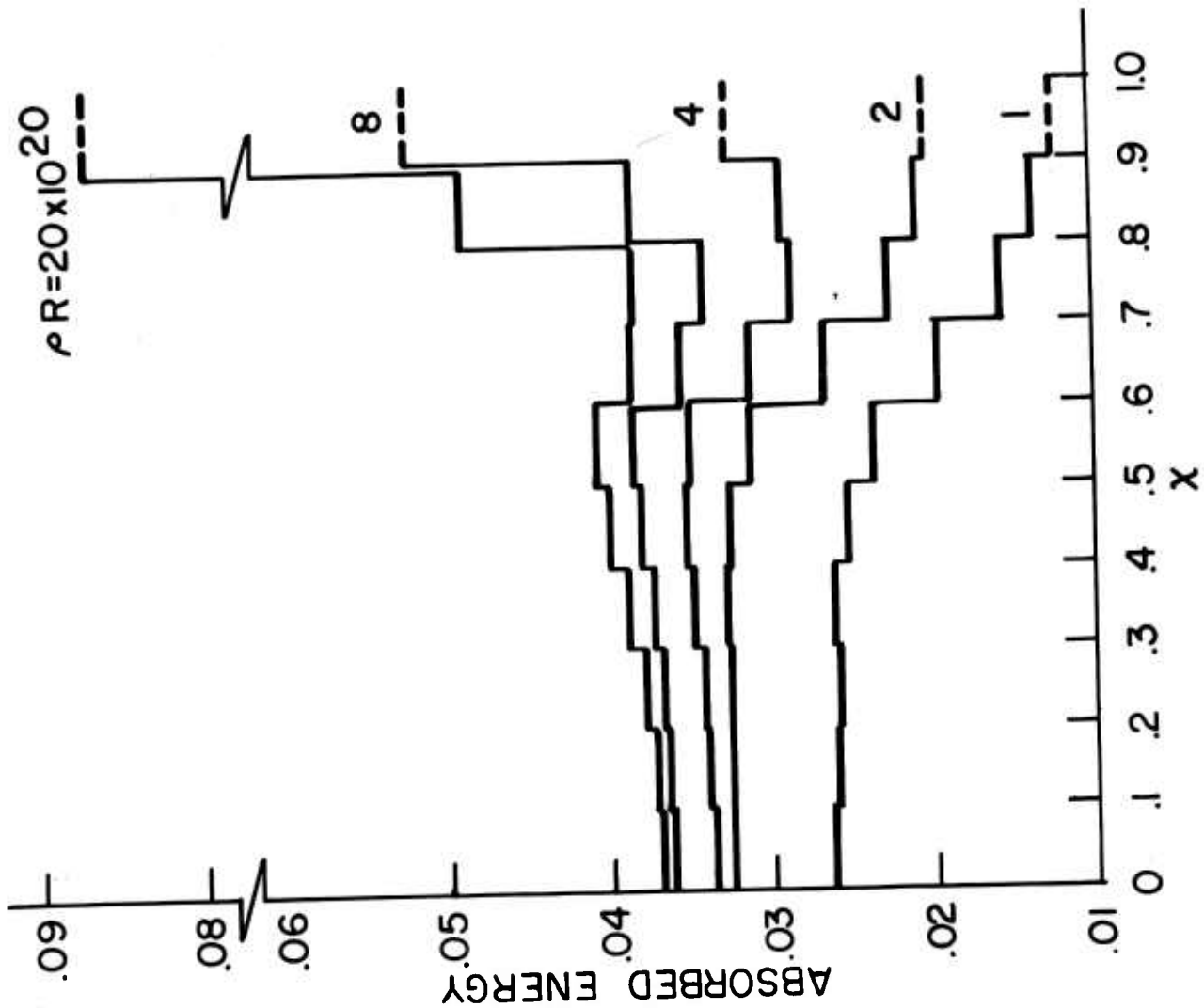

Figure 15. Absorbed Energy vs Normalized Radius in a Rod

TABLE V

Absorbed Energy per χ Interval for Code 0580 Glass

$\Delta\chi \rightarrow$ $\rho R \times 10^{-20}$	0-.1	.1-.2	.2-.3	.3-.4	.4-.5	.5-.6	.6-.7	.7-.8	.8-.9	.9-1.0
1.	.0262	.0261	.0260	.0261	.0254	.0237	.0196	.0159	.0138	.0124
$\sqrt{2}$	.0300	.0299	.0298	.0301	.0296	.0279	.0234	.0194	.0173	.0160
2.	.0324	.0324	.0324	.0328	.0326	.0313	.0267	.0228	.0210	.0203
$2\sqrt{2}$	.0323	.0323	.0325	.0329	.0331	.0324	.0284	.0252	.0245	.0253
4	.0338	.0340	.0342	.0348	.0351	.0349	.0312	.0286	.0292	.0325
$4\sqrt{2}$	.0347	.0348	.0351	.0357	.0363	.0364	.0331	.0313	.0337	.0413
8	.0362	.0364	.0367	.0373	.0380	.0384	.0353	.-340	.0383	.0521
20	.0369	.0372	.0378	.0388	.0399	.0407	.0384	.0382	.0489	.0871

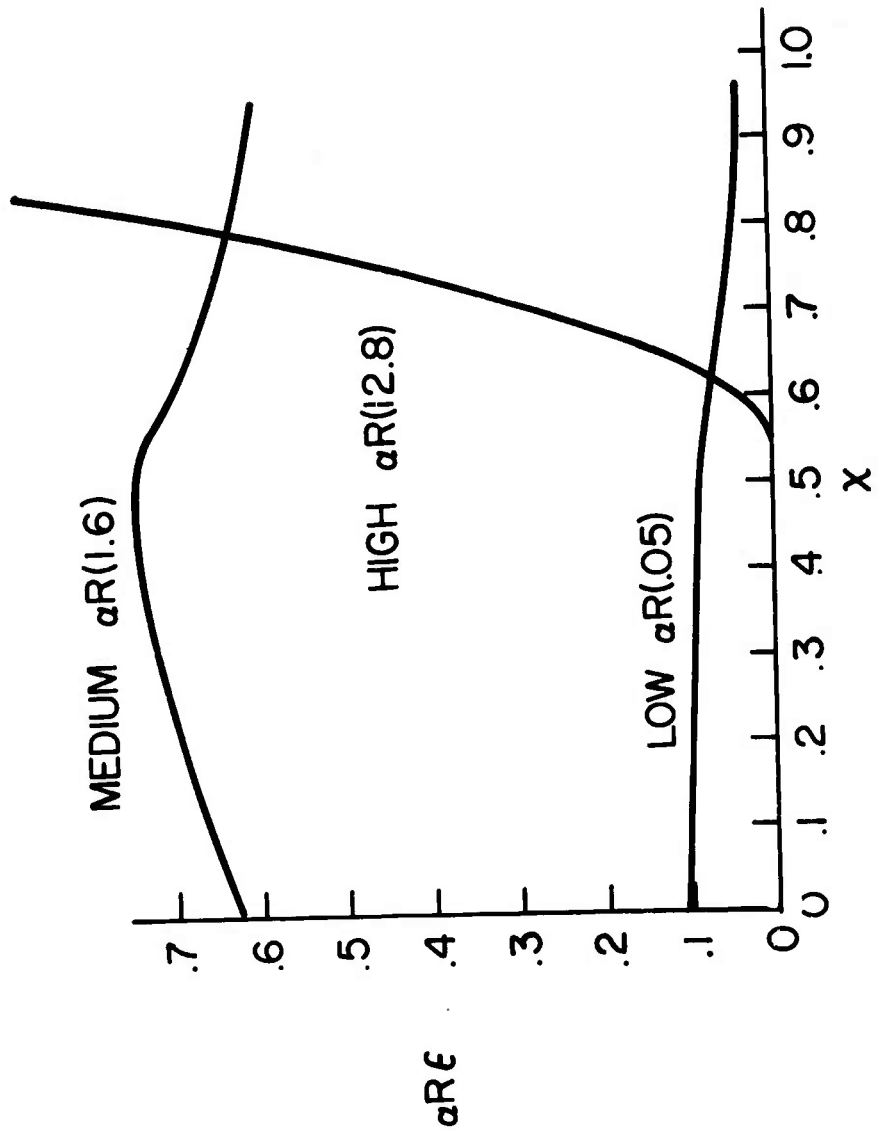

Figure 16. Energy Density Times αR vs Normalized Radius

similar to that observed for $\rho R = 2 \times 10^{-20}$ in Figure 15.

At high ρR values, contributions to the absorbed energy are made up of some small αR's, intermediate αR's and large αR's. Thus the total absorbed energy density may be thought of as a combination of all three types of terms as shown in Figure 16 with the large αR's being weighted more heavily. The resulting sum of these curves is similar to that shown in Figure 15 for $\rho R > 4\sqrt{2}$.

The curves of Figure 15 reveal several interesting facts. First, there is no particular ρR value where the energy absorbed is constant across the radius of the rod. Second, at all Nd concentrations there is appreciable pumping in the center of the rod. Third, there is no advantage, in practical devices, for ρR being greater than about 5×10^{20} ions/cc. For ρR's greater than this value most of the increase in absorbed energy is near the surface. This can cause undesireable effects, for instance: a) The surface may lase first; and b) Large thermal gradients can exist.

The programs written for these calculations are general and applicable to all homogeneous materials. Data required are the refractive index, the absorption spectrum and illumination spectrum. These calculations were based on the properties of Corning Code 0580 laser glass. Materials having similar refractive indices and absorption spectra can be expected to give similar results. The results for borate glasses may be appreciably different.

IV. REFERENCES

1) Semiannual Report for ONR Contract No. Nonr-38 33 (00) January 1964.

2) Molby, F. A., J. Optical Soc. Am. 39,600 (1949).

3) El Yashevich M. A., "Spectra of the Rare Earths," Book 2, AEC. Translation Series, 1963.

4) McClure, D. S., Solid State Physics, 9, 399 (1959).

5) Elliott, R. J. and Stevens, K. W. H., Proc, Roy. Soc. 215A, 437 (1952), 218A, 553 (1953).

6) Judd, B. R., Proc. Roy. Soc., 251A, 134 (1959), 247A, 458 (1955).

7) Borrelli, N. F. et al., Presentation to ONR March 1964, (To be published).

8) MacAvoy et al., CGW Ann. Rept. to ONR, June, 1963, (AD429 010).

9) Judd, B. R., Proc. Roy. Soc., 227A, 552 (1955).

10) VanVleck, J. H., J. Phys. Chem. 41, 67 (1936).

11) Sooy, W. R. and Stitch, M. L., J. Appl. Phys. 34, 1719 (1963).

UNCLASSIFIED